Optics Letters

Nonlinear pulse compression to 51-W average power GW-class 35-fs pulses at 2-µm wavelength in a gas-filled multi-pass cell

P. Gierschke,[1,2,*] C. Grebing,[1,3] M. Abdelaal,[2] M. Lenski,[2] J. Buldt,[2] Z. Wang,[2] T. Heuermann,[2,4,5] M. Mueller,[2,6] M. Gebhardt,[2,4,5] J. Rothhardt,[1,2,4,5] and J. Limpert[1,2,4,5]

[1]Fraunhofer Institute for Applied Optics and Precision Engineering, Albert-Einstein-Straße 7, 07745 Jena, Germany
[2]Institute of Applied Physics, Abbe Center of Photonics, Friedrich Schiller University Jena, Albert-Einstein-Straße 15, 07745 Jena, Germany
[3]Present address: Active Fiber Systems GmbH, Ernst-Ruska Ring 17, 07745 Jena, Germany
[4]Helmholtz-Institute Jena, Fröbelstieg 3, 07743 Jena, Germany
[5]GSI Helmholtzzentrum für Schwerionenforschung, Planckstraße 1, 64291 Darmstadt, Germany
[6]Present address: Institute de Physique, Université de Neuchâtel, Avenue de Bellevaux 51, 2000 Neuchâtel, Switzerland
*Corresponding author: philipp.gierschke@iof.fraunhofer.de

Received 13 May 2022; revised 7 June 2022; accepted 15 June 2022; posted 17 June 2022; published 11 July 2022

We report on the generation of GW-class peak power, 35-fs pulses at 2-µm wavelength with an average power of 51 W at 300-kHz repetition rate. A compact, krypton-filled Herriott-type cavity employing metallic mirrors is used for spectral broadening. This multi-pass compression stage enables the efficient post compression of the pulses emitted by an ultrafast coherently combined thulium-doped fiber laser system. The presented results demonstrate an excellent preservation of the input beam quality in combination with a power transmission as high as 80%. These results show that multi-pass cell based post-compression is an attractive alternative to nonlinear spectral broadening in fibers, which is commonly employed for thulium-doped and other mid-infrared ultrafast laser systems. Particularly, the average power scalability and the potential to achieve few-cycle pulse durations make this scheme highly attractive.

https://doi.org/10.1364/OL.462647

Ultrafast lasers in the short-wavelength infrared region (SWIR, ranging from 1.5 µm to 3.0 µm in wavelength) are of interest for manifold direct applications and frequency conversion techniques to terahertz, mid-infrared, or even soft and hard x-ray regions [1–3]. For example, high-harmonic generation (HHG) with table-top SWIR driving sources is a promising route to address the highly application-relevant soft x-ray (SXR) regime [4]. This spectral region which expands from approximately 280 eV to 530 eV, known as the "water window", is of utmost interest in high-resolution imaging or extreme ultraviolet (XUV)-spectroscopy of biological specimen [5]. These and other applications emphasize the demand for scalable, high-flux, table-top SXR HHG sources. To push the spectral coverage of laser-driven HHG sources beyond the carbon K-edge (~284 eV), the SWIR has been identified as a favorable driving wavelength region to exploit the increasing phase-matching photon energy cutoff with longer laser wavelength [6]. At the same time, this wavelength regime balances the increased cutoff in the water window with a reasonable single-atom response [7]. Additionally, employing few-cycle driving pulses in the HHG process ensures that high phase-matching peak intensities can be used, before excessive ionization spoils the transient phase-matching at the temporal peak of the pulse [8]. Furthermore, such few-cycle pulses facilitate the generation of isolated attosecond pulses in the SXR region [9]. In addition to the above considerations, compensating the reduced long-wavelength-driven HHG efficiency, with high input average power to optimize the overall photon flux of the coherent SXR radiation, has been one of the main goals within the ultrafast laser development community. Recently, optical parametric chirped-pulse amplification (OPCPA) has been established as a concept to provide the high average power few-cycle SWIR HHG driving pulses [10,11]. Such bulk-crystal-based systems are typically driven by 1.0-µm (up to kW-class average power) pump sources and emit average powers of several tens of watts. Another concept aimed at high-power, high-efficiency few-cycle pulse generation in the SWIR is based on a scalable ultrafast laser concept using active gain media such as holmium-doped materials [12] or thulium-doped fiber chirped-pulse amplification systems (Tm:FCPA) [13,14]. Thulium-based systems provide multi-GW peak powers, multi-100-W average output power, and can indeed support pulses as short as sub-100 fs. Nevertheless, a subsequent pulse shortening according to the abovementioned discussion is typically desired. Hence, an efficient and high-power capable pulse post-compression is of high importance. Nonlinear pulse compression in the SWIR spectral region is traditionally done in waveguides such as noble-gas-filled capillaries [15,16]. While reaching millijoule-class few-cycle pulses, the throughput efficiency of such systems is fundamentally limited by the capillary propagation loss. Most recently, the pulse compression of a 50-W average power Tm:FCPA system and simultaneous high-flux high harmonic generation toward the SXR region in a helium-filled anti-resonant hollow-core fiber have been demonstrated [17]. In addition to fiber-based post-compression schemes, multi-pass cells (MPC) have emerged

as an attractive approach for nonlinear post-compression providing high throughput efficiency, compact footprints, excellent beam quality, and a spatially homogenized spectral broadening [18–20]. At near-infrared wavelengths, compressed average powers as high as 1 kW [21], pulse durations as short as <7 fs at high peak powers [22], and pulse energies above 100 mJ have been reported [23], highlighting the capabilities of this concept. Until now, MPCs have rarely been demonstrated in the SWIR wavelength regime. To date, a pulse compression at 1550-nm wavelength with approximately 2-W average power [24] and nonlinear spectral broadening at 2.05 µm of 1.74-mJ 1.43-ps pulses to 270 fs with excellent efficiency has been demonstrated [25].

In this Letter, we report on the first nonlinear post-compression of the output of a Tm:FCPA in a gas-filled MPC. The driving laser system (Active Fiber Systems GmbH) delivers 138-fs pulses (FWHM) and 65 W of average output power at a repetition rate of 300 kHz, centered at a wavelength of 1940 nm. A beam quality factor of $M^2 \leq 1.2$, an excellent long-term pointing stability of <10 µrad rms, and <0.1% rms average power variation over 8 hours, make this system an ideal platform to drive a multitude of applications. Approximately 72% of the energy (158 µJ) is contained in the main feature of the CPA output pulse, a value validated by second-order frequency-resolved optical gating (SHG-FROG). Consequently, the peak power relevant to experiments driven by this laser is approximately 1.2 GW. As depicted in Fig. 1, the post-compression stage consists of a Herriott-type cavity comprising two concave, dielectrically enhanced silver-coated silicon mirrors. The substrate material of the mirrors was chosen due to its low expansion and high heat conductivity. The coating is optimized for the driving wavelength ($R_{avg} > 99\%$, |group delay dispersion (GDD)| < 30 fs^2, 1600–2300 nm) and was designed to support the bandwidth of few-cycle pulses (<20 fs) at a center wavelength of approximately 2 µm. For this reason, no highly reflective dielectric multilayer coatings were used. The radius of curvature of these 2" (50.4 mm) mirrors is 100 mm and the resonator length is chosen to be 196 mm, forming a nearly concentric cavity close to the stability edge. The input is matched to the resonator eigenmode using an antireflective-coated lens with a focal length of 150 mm. The theoretical Gaussian eigenmode at a center wavelength of 1940 nm has $1/e^2$ diameters of 1.4 mm and 0.18 mm at the mirror surface and the focal position, respectively. The MPC design takes two limitations into account. First, ionization-induced disturbance of the beam at the focus defined by a limit peak intensity I_{ion} above which the ionization rate of the gas medium is too high to ensure proper operation. Therefore, the peak intensity for ionization is limited to values satisfying $I_{ion} > 2E_{in}/\pi w_0^2 \tau_{in}$, where E_{in} is the input pulse energy, w_0^2 the cavity waist radius, and τ_{in} the input pulse duration. The resulting peak intensity in this experiment corresponds to 5×10^{12} W/cm^2 and is below the ionization threshold intensity (1.3×10^{13} W/cm^2) for krypton, which is the gas of choice for the experiments discussed herein. This intensity corresponds to well over 10^3 times stronger index perturbation from the Kerr effect as compared to that associated with plasma formation. The ionization rates relevant to this evaluation are calculated via the Yudin–Ivanov formula [26]. The second limitation is optical damage of the MPC mirrors. The peak fluence on the mirror surface (0.03 J/cm^2) is kept below 0.1 J/cm^2 to strictly avoid mirror damage. Hence, these design features provide a sufficient safety margin for both limitations and ensure reliable long-term operation. For in- and outcoupling of the beam, two scraper mirrors consisting of gold coated silicon substrates are placed in front of each cavity mirror. After 12 round trips, the power transmission is still as high as 80% and the beam exits the cavity before it is sampled for diagnostics. The MPC setup is placed inside a compact vessel (45 cm × 35 cm), which allows operation at vacuum and at absolute pressures up to 3 bar. Prior to the experiment, the chamber is evacuated to high vacuum levels to reduce the amount of residual water vapor, as even small amounts of residual humidity can severely deteriorate the spatial and temporal characteristics of the propagating pulses [27], especially at high pressure of the surrounding gas [28]. To provide sufficient nonlinearity, krypton gas with a nonlinear index of $n_2 = 2.7 \times 10^{-23}$ m^2/W at 1 atm [29] is chosen. Using this nonlinear medium, the laser spectrum is broadened based on self-phase-modulation. When running the experiment under maximum pressure handling capabilities and therefore, with a pressure of $p = 3$ bar krypton, we expect a nonlinear phase shift per focal pass of $\phi_{\mathrm{nl-focus}} \sim 0.31$ rad (averaged over the transverse beam profile, based on analytical scaling laws [18], using the known laser input parameters). The critical peak power to trigger self-focusing corresponds in this configuration to approximately 6 GW, and still indicates a safe operation regime. Furthermore, the propagation can be considered dispersion free at all points during the spectral broadening, since the dispersion length after the last focal pass L_d (~60 m) is still much longer than the residual propagation path L_{prop} (~0.5 m) [30]. Hence, the pulse duration is not changing significantly during propagation. The total phase shift is expected to be $\phi_{\mathrm{nl-total}} = \phi_{\mathrm{nl-focus}} \times n_{\mathrm{foci}} \approx 7.1$ rad after 23 focal passes leading to a theoretical compression factor of $\frac{\tau_{in}}{\tau_{out}} = \frac{\phi_{\mathrm{nl-total}}}{\sqrt{e}} = 4.3$, under assumption of a Gaussian pulse shape [31]. A Fourier-limited (FL) pulse duration of 32 fs is expected. As depicted in Fig. 1, the output beam of the MPC is sampled with a wedge, directing the front reflection to the beam diagnostics (SHG-FROG, spectrum, beam quality) and the transmitted beam to a thermal power sensor. The output average power of the MPC at the above-described conditions is 51 W, corresponding to a 170-µJ pulse energy. The throughput of the MPC is approximately 80%, which is close to the theoretical value (82%). At this performance level, the measured input 30-dB bandwidth (120 nm) is increased to more than 400 nm (both spectra are depicted in Fig. 2). The measured spectral broadening corresponds reasonably well to the

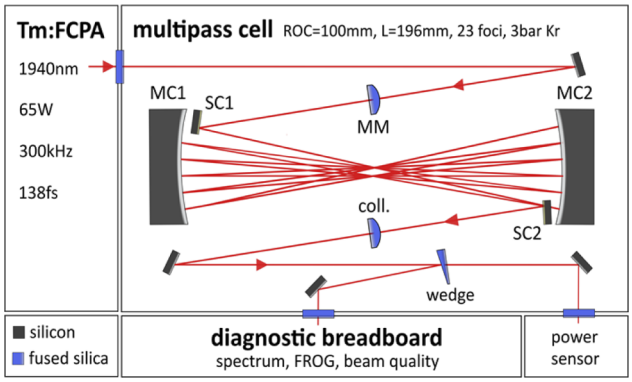

Fig. 1. Schematic of the experimental setup. Tm:FCPA, thulium-doped fiber chirped-pulse amplifier; MC, cavity mirror; ROC, cavity mirror radius of curvature; L, cavity mirror distance; SC, scraper mirror; MM, mode matching lens (focal length = 150 mm).

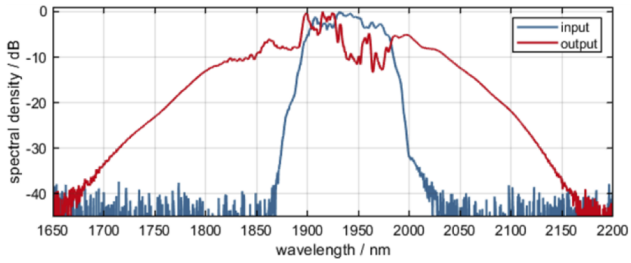

Fig. 2. Measured input (blue line) and broadened output spectrum.

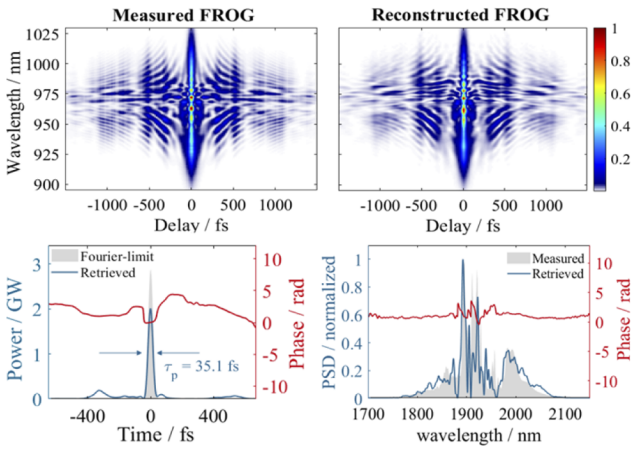

Fig. 3. FROG measurement of the compressed output. Top graphs: Measured (left) and reconstructed (right) FROG trace. Bottom (left): Retrieved pulse and corresponding Fourier-limit. Bottom (right): Measured and retrieved spectrum of the MPC output.

expected temporal compression factor as discussed above, supporting an FL pulse duration of 34 fs. Exploiting the anomalous dispersion of fused silica at a wavelength of 1940 nm (group velocity dispersion (GVD) ~ −88 fs^2/mm [32]), the compression can be performed with fused silica. The pulses are already partially compressed after transmission through the output windows of the MPC. The residual chirp of the beam sample is removed by passing another uncoated fused silica wedge outside the MPC. In both output ports (see Fig. 1), the amount of transmission through fused silica is the same. The total GDD corresponds to approximately −1700 fs^2. To analyze the compressed output, an in-house built SHG-FROG is employed. The corresponding results are shown in Fig. 3. For the reconstruction, a ptychography algorithm [33] is used with a quadratic grid size of 1024 × 1024 points. The reconstructed spectrum matches well with the measured data, supported by the FROG reconstruction error of <0.1% rms. The retrieved FWHM duration of the compressed pulses is 35.1 fs and therewith close to the Fourier limit of the measured spectrum. Owing to the fact that a 158-μJ input pulse energy contributes to the nonlinear propagation in the cell, the compressed SWIR pulse contains 122 μJ. Normalizing the energy of the reconstructed pulse to this value yields an achievable peak power of approximately 2 GW. Please note that the temporal characterization is realized with the sampled beam, however, the identical amount of dispersion material (fused silica) is placed in the beam path toward the power meter. The beam quality has been measured and evaluated according to the ISO 11146-1:2021 norm using a high-sensitivity indium–antimonide chip-based camera. The

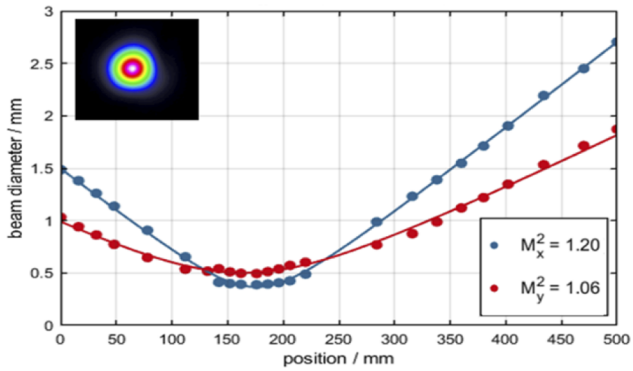

Fig. 4. Measurement results of the M^2 value of the MPC output according to ISO 11146-1:2021. A close to diffraction-limited beam quality is revealed. The focused beam profile is depicted in the inset.

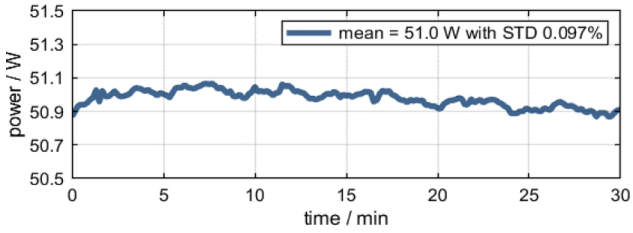

Fig. 5. Long-term measurement of the MPC output power using a thermal power sensor and sampling rate of 5 s.

recorded images are background corrected and a beam diameter evaluation according to the 4 σ-Method is performed. The results are depicted in Fig. 4, showing a close to diffraction-limited beam quality in both axes, characterized by an $M^2 \leq 1.2$ (input beam, $M^2 \leq 1.2$). The small off-set between the two axes can be addressed to slight beam astigmatism which is also present at the input beam. These measurements confirm that the nonlinear broadening preserves the beam quality of the input beam. To identify that there are no immediate thermal drifts on a time scale of several minutes, we investigate the average output power stability of the MPC over half an hour. The output power was logged using a thermal power sensor with a sampling rate of 5 s. The result is depicted in Fig. 5 showing a high stability with a mean value of 51 W and a standard deviation below 0.1% over the captured time span (input beam power stability, <0.1%). The spectral broadening in this experiment was limited due to the maximum applicable pressure of 3 bar to the vessel. Since the metallic mirrors support significantly broader spectra, a larger compression factor is conceivable by applying a higher gas pressure. According to numerical simulation, increasing the gas pressure to 4 bar within a suitable high-pressure vessel, a spectrum which supports few cycle pulses could be achieved (while simultaneously keeping all other parameters constant). The corresponding critical peak power for self-focusing is then 4.9 GW and still indicates a reasonable operation regime without strong spatio-spectral couplings. Following the calculation on the accumulated B-integral as mentioned earlier, a total average phase shift of ~11 rad and therefore a compression factor of approximately 7, leading to a sub-20-fs pulse duration, is expected. If the phase shift per individual pass can be increased even further by approaching the self-focusing limit, higher transmission can be achieved by reducing the number of round trips.

In conclusion, we have demonstrated the first high average power gas-filled multi-pass cell-based post-compression in the SWIR wavelength region. The MPC delivers an average output power of 51 W with pulses as short as 35 fs, at a repetition rate of 300 kHz. The emission is characterized by an excellent power stability and a close to diffraction-limited beam quality of $M^2 \leq 1.2$. This was possible even without external cooling of the cavity optics.

Further average power scaling to several 100 W seems feasible by applying direct water-cooling on the silicon substrates, as has already been experimentally demonstrated in [22]. The overall setup is very compact and easily implemented at the output of the ultrafast 2-µm wavelength source. The presented system renders an ideal platform to drive nonlinear frequency conversion experiments into the soft x-ray region via HHG, because it simultaneously delivers high average and high peak powers in the SWIR wavelength region. Further power scaling as well as further broadening seems feasible by applying a suitable high-pressure chamber and larger cavity designs. We believe that average powers beyond 100 W, millijoule pulse energies, and few-cycle duration can be demonstrated in the near future, using MPC-based post-compression schemes of SWIR ultrafast lasers.

Funding. Fraunhofer Cluster of Excellence Advanced Photon Sources (CAPS); H2020 European Research Council ("SALT", 835306); Innovation Pool of the Research Field Matter of the Helmholtz Association of German Research Centers (project FISCOV); Thüringer Ministerium für Bildung, Wissenschaft und Kultur (2017 FGR 0076, 501100004404); Thüringer Aufbaubank (Forschergruppe 2015FGR0094); Helmholtz Association (grant agreement HGF ExNet-0019-Phase 2–3).

Disclosures. The authors declare no conflicts of interest.

Data availability. Data underlying the results presented in this paper are not publicly available at this time but may be obtained from the authors upon reasonable request.

REFERENCES

1. M. Clerici, M. Peccianti, B. E. Schmidt, L. Caspani, M. Shalaby, M. Giguère, A. Lotti, A. Couairon, F. Légaré, T. Ozaki, D. Faccio, and R. Morandotti, Phys. Rev. Lett. **110**, 253901 (2013).
2. J. Zhang, K. Fai Mak, N. Nagl, M. Seidel, D. Bauer, D. Sutter, V. Pervak, F. Krausz, and O. Pronin, Light: Sci. Appl. **7**, 17180 (2018).
3. A. Koç, C. Hauf, M. Woerner, L. von Grafenstein, D. Ueberschaer, M. Bock, U. Griebner, and T. Elsaesser, Opt. Lett. **46**, 210 (2021).
4. S. L. Cousin, F. Silva, S. Teichmann, M. Hemmer, B. Buades, and J. Biegert, Opt. Lett. **39**, 5383 (2014).
5. Y. Fu, K. Nishimura, R. Shao, A. Suda, K. Midorikawa, P. Lan, and E. J. Takahashi, Commun. Phys. **3**, 92 (2020).
6. T. Popmintchev, M. C. Chen, A. Bahabad, M. Gerrity, P. Sidorenko, O. Cohen, I. P. Christov, M. M. Murnane, and H. C. Kapteyn, Proc. Natl. Acad. Sci. U. S. A. **106**, 10516 (2009).
7. A. D. Shiner, C. Trallero-Herrero, N. Kajumba, H. C. Bandulet, D. Comtois, F. Légaré, M. Giguère, J. C. Kieffer, P. B. Corkum, and D. M. Villeneuve, Phys. Rev. Lett. **103**, 073902 (2009).
8. B. E. Schmidt, A. D. Shiner, M. Giguère, P. Lassonde, C. A. Trallero-Herrero, J. C. Kieffer, P. B. Corkum, D. M. Villeneuve, and F. Légaré, J. Phys. B: At., Mol. Opt. Phys. **45**, 074008 (2012).
9. J. Li, X. Ren, Y. Yin, K. Zhao, A. Chew, Y. Cheng, E. Cunningham, Y. Wang, S. Hu, Y. Wu, M. Chini, and Z. Chang, Nat. Commun. **8**, 186 (2017).
10. M. K. R. Windeler, K. Mecseki, A. Miahnahri, J. S. Robinson, J. M. Fraser, A. R. Fry, and F. Tavella, Opt. Lett. **44**, 4287 (2019).
11. T. Feng, A. Heilmann, M. Bock, L. Ehrentraut, T. Witting, H. Yu, H. Stiel, S. Eisebitt, and M. Schnürer, Opt. Express **28**, 8724 (2020).
12. S. Tomilov, Y. Wang, M. Hoffmann, J. Heidrich, M. Golling, U. Keller, and C. J. Saraceno, "50-W average power Ho:YAG SESAM-modelocked thin-disk oscillator at 2.1 um," ArXiv:2204.01340 (2022).
13. T. Heuermann, Z. Wang, M. Lenski, M. Gebhardt, C. Gaida, M. Abdelaal, J. Buldt, M. Müller, A. Klenke, and J. Limpert, Opt. Lett. **47**, 3095 (2022).
14. C. Gaida, M. Gebhardt, T. Heuermann, F. Stutzki, C. Jauregui, and J. Limpert, Opt. Lett. **43**, 5853 (2018).
15. T. Balciunas, C. Fourcade-Dutin, G. Fan, T. Witting, A. A. Voronin, A. M. Zheltikov, F. Gerome, G. G. Paulus, A. Baltuska, and F. Benabid, Nat. Commun. **6**, 6117 (2015).
16. V. Cardin, N. Thiré, S. Beaulieu, V. Wanie, F. Légaré, and B. E. Schmidt, Appl. Phys. Lett. **107**, 181101 (2015).
17. M. Gebhardt, T. Heuermann, R. Klas, C. Liu, A. Kirsche, M. Lenski, Z. Wang, C. Gaida, J. E. Antonio-Lopez, A. Schülzgen, R. Amezcua-Correa, J. Rothhardt, and J. Limpert, Light: Sci. Appl. **10**, 36 (2021).
18. M. Hanna, X. Délen, L. Lavenu, F. Guichard, Y. Zaouter, F. Druon, and P. Georges, J. Opt. Soc. Am. B **34**, 1340 (2017).
19. A. Viotti, M. Seidel, E. Escoto, S. Rajhans, W. P. Leemans, I. Hartl, and C. M. Heyl, Optica **9**, 197 (2022).
20. Y. Pfaff, C. Forster, G. Barbiero, M. Rampp, S. Klingbeil, J. Brons, C. Y. Teisset, H. Wang, R. Jung, J. Jaksic, A. H. Woldegeorgis, C. J. Saraceno, and T. Metzger, Opt. Express **30**, 10981 (2022).
21. C. Grebing, M. Müller, J. Buldt, H. Stark, and J. Limpert, Opt. Lett. **45**, 6250 (2020).
22. M. Müller, J. Buldt, H. Stark, C. Grebing, and J. Limpert, Opt. Lett. **46**, 2678 (2021).
23. M. Kaumanns, D. Kormin, T. Nubbemeyer, V. Pervak, and S. Karsch, Opt. Lett. **46**, 929 (2021).
24. G. Jargot, N. Daher, L. Lavenu, X. Delen, N. Forget, M. Hanna, and P. Georges, Opt. Lett. **43**, 5643 (2018).
25. H. Cankaya, K. Fritsch, C. Mahnke, C. Vidoli, I. Hartl, F. Kaertner, and O. Pronin, in *Conference on Lasers and Electro-Optics (CLEO)* (2022), JM2E.2.
26. G. L. Yudin and M. Y. Ivanov, Phys. Rev. A: At., Mol., Opt. Phys. **64**, 4 (2001).
27. M. Gebhardt, C. Gaida, F. Stutzki, S. Hädrich, C. Jauregui, J. Limpert, and A. Tünnermann, Opt. Express **23**, 13776 (2015).
28. M. Gebhardt, C. Gaida, F. Stutzki, S. Hädrich, C. Jauregui, J. Limpert, and A. Tünnermann, Opt. Lett. **42**, 747 (2017).
29. C. Brée, A. Demircan, and G. Steinmeyer, Phys. Rev. A **85**, 033806 (2012).
30. G. P. Agrawal, *Nonlinear Fiber Optics* (Elsevier, 2013).
31. R. M. Kaumanns, "Generation of energetic femtosecond pulses at high average power," Ph.D. thesis (Ludwig Maximilian University of Munich, 2020).
32. I. H. Malitson, J. Opt. Soc. Am. **55**, 1205 (1965).
33. P. Sidorenko, O. Lahav, Z. Avnat, and O. Cohen, Optica **4**, 1388 (2017).